HOKKAIDO UNIVERSITY

Title	Bioimaging of Pb and STIM1 in mice liver, kidney and brain using Laser Ablation Inductively Coupled Plasma Mass Spectrometry (LA-ICP-MS) and immunohistochemistry
Author(s)	Togao, Masao; Nakayama, Shouta M. M.; Ikenaka, Yoshinori et al.
Citation	Chemosphere, 238, 124581 https://doi.org/10.1016/j.chemosphere.2019.124581
Issue Date	2020-01-01
Doc URL	https://hdl.handle.net/2115/83751
Rights	© 2020. This manuscript version is made available under the CC-BY-NC-ND 4.0 license https://creativecommons.org/licenses/by-nc-nd/4.0/
Rights(URL)	https://creativecommons.org/licenses/by-nc-nd/4.0/
Type	journal article
File Information	Manuscript.pdf

Hokkaido University Collection of Scholarly and Academic Papers : HUSCAP

Title

Bioimaging of Pb and STIM1 in mice liver, kidney and brain using Laser Ablation Inductively Coupled Plasma Mass Spectrometry (LA-ICP-MS) and immunohistochemistry

Short title

Bioimaging of Pb and STIM1 in mice liver, kidney and brain

Author names

Masao Togao [1, a)], Shouta M.M. Nakayama [1, a)], Yoshinori Ikenaka [1, 2)], Hazuki Mizukawa [3)], Yoshiki Makino [4)], Ayano Kubota [5)], Takehisa Matsukawa [5)], Kazuhito Yokoyama [5)], Takafumi Hirata [6)], Mayumi Ishizuka [1, *)]

Authors' affiliation

(1) Laboratory of Toxicology, Department of Environmental Veterinary Sciences, Graduate School of Veterinary Medicine, Hokkaido University, Kita 18 Nishi 9, Kita-ku, Sapporo 060-0818, Japan

(2) Water Research Group, School of Environmental Sciences and development, North-West University, South Africa

(3) Department of Science and Technology for Biological Resources and Environment, Graduate School of Agriculture, Ehime University, Tarumi 3-5-7, Matsuyama, Ehime, 790-8566 Japan

(4) Division of Earth and Planetary Sciences, Kyoto University, Kyoto, Japan

(5) Department of Epidemiology and Environmental Health, Juntendo University Faculty of Medicine, Tokyo, Japan

(6) Graduate School of Science, The University of Tokyo, Tokyo, Japan

(a) Both authors equally contributed to this study (Dual first authorship).

Authors' e-mail address:

Masao Togao <togamasa12@gmail.com>

Shouta M.M. Nakayama <shouta-nakayama@vetmed.hokudai.ac.jp>

Yoshinori Ikenaka <y_ikenaka@vetmed.hokudai.ac.jp>

Hazuki Mizukawa <hazuki.mizukawa@vetmed.hokudai.ac.jp>

Yoshiki Makino <y.makino.kueps@gmail.com>

Ayano Kubota <ay-kubota@juntendo.ac.jp>

Takehisa Matsukawa <tmatsuka@juntendo.ac.jp>
Kazuhito Yokoyama <kyokoya@juntendo.ac.jp>
Takafumi Hirata <hrt1@eqchem.s.u-tokyo.ac.jp>
Mayumi Ishizuka <ishizum@vetmed.hokudai.ac.jp>

***Corresponding author:**
Mayumi ISHIZUKA
E-mail: ishizum@vetmed.hokudai.ac.jp
Laboratory of Toxicology, Department of Environmental Veterinary Sciences, Graduate School of Veterinary Medicine, Hokkaido University, N18, W9, Kita-ku, Sapporo 060-0818, Japan
Tel: +81-11-706-6949; Fax: +81-11-706-510

Abstract

Lead (Pb) pollution is one of the most serious environmental problems and has attracted worldwide attention. Pb causes hematological, central nervous system, as well as renal toxicity, and so on. Although many investigations about Pb in blood to evaluate pollution status and toxic effects have been reported, there are open question about biological behavior of Pb. In order to reveal any toxicological mechanisms or influences, we focused on the local distribution of Pb in mice organs. Lead acetate (100 mg/L and 1,000 mg/L) in drinking water were given to the BALB/c mice (male, seven weeks of age, N = 24) for three weeks. Laser Ablation Inductively Coupled Plasma Mass Spectrometry (LA-ICP-MS) analysis revealed a homogenous distribution of Pb in the liver and inhomogeneous distribution in the kidney and brain. The hippocampus, thalamus, and hypothalamus had higher concentrations than other areas such as the white matter. Surprisingly, in the kidney, Pb tended to accumulate in the medulla rather than the cortex, strongly suggesting that high sensitivity areas and high accumulation areas differ. Moreover, distribution of stromal interacting protein 1 which is candidate gene of Pb pathway to the cells was homogenous in the liver and kidney whereas inhomogeneous in the brain. In contrast to our hypothesis, interestingly, Pb exposure under the current condition did not induce mRNA expressions for any candidate channel or transporter genes. Thus, further study should be conducted to elucidate the local distribution of Pb and other toxic metals, and pathway that Pb takes to the cells.

Keywords

Cell entry mechanisms

Laser Ablation Inductively Coupled Plasma Mass Spectrometry (LA-ICP-MS)

Distribution

Pb

Stromal interacting protein 1 (STIM1)

1. Introduction

Elemental analysis of biological samples including internal organs are mainly conducted by atomic absorption spectrometry (AAS; Yabe et al., 2012), Inductively coupled plasma-atomic emission spectrometry (ICP-OES; Rahil-Khazen et al., 2002), and inductively coupled plasma-mass spectrometry (ICP-MS; Nakata et al., 2016). Usually, liquid samples are analyzed by such techniques, therefore organs are acid digested and there is an assumption that they contain a homogeneous distribution of investigated element (Konz et al., 2012). However, it is unknown about distribution patterns of elements such as Pb, Cd and Hg in organs. If they are inhomogeneously distributed, the evaluation of their concentrations in organs should be reconsidered.

Elemental analysis using ICP-MS combined with laser ablation (LA) has been conducted (Pozebon et al., 2014, Noël et al., 2015, Yamashita et al., 2019). A solid surface of sample is ablated by a pulse laser beam in the laser ablation chamber, the ablated material is then analyzed by ICP-MS. Scanning of the surface by LA allows the construction of images of elements distribution (Becker et al., 2010, Yamashita et al., 2019). This method allows direct analysis of solid sample surfaces and is applicable for thin organ slices (Becker et al., 2005, 2010, Ishii et al., 2018, Limbeck et al., 2015). Numerous studies have used this method to analyze the local distribution of essential elements such as Cu, Fe, and Zn in organs, bones and teeth in human and animals (Becker et al., 2015, Ishii et al., 2018, Johnston et al., 2019, Paul et al., 2015, Urgast et al., 2012). However, with regards to Pb, there is still less published research which investigate distribution in organs and bones (Dobrowolska et al., 2008, Ishii et al., 2018, Johnston et al., 2019). Dobrowolska et al. (2008) showed a homogeneous Pb distribution in brain regions. However, they analyzed the human brain (postmortem from a healthy donor) and found very low Pb levels. Ishii et al. (2018) revealed the

distribution of Pb in bone of raptor species. To our best knowledge, there has not yet been any research using Pb administrated laboratory animals (e.g. mice models) to elucidate the local distribution of Pb in internal organs.

Despite various research efforts, the pathway by which Pb enters cells remains unclear; this is still one of the important points concerning Pb toxicity (Chang et al., 2008, Zhang et al., 2014). Pb^{2+} has the ability to mimic Ca^{2+} and other divalent metal ions such as Fe^{2+} and Zn^{2+} (Zhang et al., 2014). Based on this mimicry, Ca^{2+} and other divalent metal channels might be candidates for Pb entry (Godwin 2001). Two types of Ca^{2+} channels: voltage gated Ca^{2+} channels (VGCCs) and store operated Ca^{2+} channels (SOCs), have been identified as potential routes by which Pb can enter cells (Kerper and Hinkle 1997). With regards to VGCCs, this would only be feasible for excitable cells. However, Pb may enter not only excitable cells but also other cells such as human embryonic kidney cell 293 (Zhang et al., 2014, Chiu et al., 2009). Thus, VGCCs may still provide a pathway to cells, but there must also be an additional route by which Pb enters the cells in the rest of the body.

Some researchers have proposed that SOCs may play an important role in Pb entry into cells (Chang et al., 2008, Kerper and Hinkle 1997, Chiu et al., 2009). SOCs are constituted from transient receptor potentials (TRPs) and Orai1 present in the plasma membrane, as well as from stromal interacting protein 1 (STIM1) present in the endoplasmic reticulum (ER) membrane (Chang et al., 2008, Zhang et al., 2014, Chiu et al., 2009).

Researchers have shown that STIM1 can translocate to interact with both Orai1 and TRPC1 during the activation of SOCs (Cheng et al., 2008, Liao et al., 2008). Although some research has indicated that STIM1 may be a key protein by which Pb

97 enters the cell (Chang et al., 2008, Chiu et al., 2009), and may contribute to the
98 localization of STIM1 (Klejman et al., 2009, Skibinska-Kijek et al., 2009), no studies
99 have compared local distribution of Pb with that of STIM1. Additionally, to our
100 knowledge, no studies have yet confirmed whether Pb induces STIM1.

101 In view of the above, we conducted an experiment using mice to achieve the
102 following aims: (1) to demonstrate the local distribution of Pb in organs; (2) to compare
103 the distribution of STIM1 with that of Pb; and (3) to clarify whether Pb induces STIM1.
104

2. Materials and methods

2.1. Animals

BALB/c mice (male, seven weeks of age, N = 24) were purchased from Sankyo Labo Service Corporation, Inc. (Tokyo, Japan). The mice were divided into three groups and housed in six polypropylene cages (N = 4 per batch). One batch from each group (control, low, and high) was sampled for ICP-MS, and the other batch from each group for LA-ICP-MS. There was no significant difference in body weight between groups (supplementary Figure S1). The animals were allowed to acclimate to the animal facilities at the Graduate School of Veterinary Medicine, Hokkaido University for one week prior to testing. Under these conditions, food (rodent chow, Labo MR Stock, Nosan Corporation, Yokohama, Japan) and distilled water were provided *ad libitum*. After acclimation, two different concentrations of lead acetate: 100 mg/L and 1,000 mg/L (Wako Pure Chemical Industries, Osaka, Japan) were given to two of the groups (the low and high dosage groups, respectively) in the drinking water for three more weeks. In our preliminary experiment, dose dependent increase of Pb concentration in blood and organs were observed when we selected 100 mg/L and 1,000 mg/L for three weeks of exposure (data not shown). The control groups were provided with distilled water. After three weeks of exposure, mice were anesthetized with sevoflurane and blood and organs (liver, kidney, and brain) were collected via the following methods. For the ICP-MS groups, blood and organ samples were collected in polypropylene tubes, then stored at -80°C in a deep freezer. For the LA-ICP-MS groups, organ samples were embedded in Tissue-Tec OCT (Sakura Finetek, CA, USA), quickly frozen in isopentane which had been cooled with dry ice, then stored at -80°C in a deep freezer. Additionally, small pieces of the liver, kidney, and brain samples were collected together with

RNAlater Tissue Storage and RNA Stabilization Solution (Sigma-Aldrich, MO, USA) in polypropylene tubes and stored at -80°C in a deep freezer for real time PCR and microarray analysis. All experiments using animals were performed under the supervision and with the approval of the Institutional Animal Care and Use Committee of Hokkaido University, Japan (approval number: 16-0017, approval day: 29th March 2016).

2.2. Quantitative analysis by ICP-MS

The ICP-MS groups were used for the quantitative analysis of Pb concentration. In this case, blood, liver, kidney, and brain were acid digested using the method described by Nakata et al. (2016, 2015) with minor modifications. The whole kidney, liver, and brain samples were dried for 48 hours in an oven at 50°C. Then, 0.1 mL of the blood samples and approximately 0.1 g of the dried biological samples were weighted and placed in pre-washed digestion vessels. This was followed by acid digestion using 5 mL of nitric acid (atomic absorption spectrometry grade, 30%; Kanto Chemical, Tokyo, Japan), and 1 mL of hydrogen peroxide (Cica reagent, 30%; Kanto Chemical). The digestion vessels subsequently underwent a ramped temperature program in a closed microwave system (Speed Wave MWS-2 microwave digestion system; Berghof, Eningen, Germany). The operating conditions of microwave system are given in the supplementary Table S1. After cooling, the sample solutions were transferred into 15 mL polypropylene tubes and diluted to a final volume of 10 mL with bi-distilled and de-ionized water (Milli-Q).

The Pb concentrations determination was performed using the procedure described by Nakata et al. (2016, 2015) with minor modifications. Concentration of Pb

was measured by ICP-MS (7700 series; Agilent Technologies, Tokyo, Japan). The operating conditions of ICP-MS are given in the supplementary Table S2. Quality control was conducted by analysis of DORM-3 (fish protein; National Research Council of Canada, Ottawa, Canada) and DOLT-4 (dogfish liver; National Research Council of Canada) certified reference materials. Replicate analysis of these reference materials showed good recovery rates (95–105%); the instrument detection limit for Pb was 0.001 µg/L.

2.3. Analysis by LA-ICP-MS

Sections of embedded liver, kidney, and brain were cut on a cryostat to a thickness of 20 µm. The native cryosections were then mounted directly onto glass slides. Then, they were analyzed using an LA system (NWR213; esi Japan, Tokyo, Japan) associated with an ICP-MS instrument (8800 series; Agilent Technologies, Tokyo, Japan). The tissue sections were systematically scanned by a focused laser beam (line by line: spot size 100 µm, scan speed 100 µm/sec, scan step 100 µm). Measured isotope (dwell time, sec) were as follows; ^{13}C (0.005), ^{25}Mg (0.005), ^{31}P (0.005), ^{43}Ca (0.005), ^{55}Mn (0.005), ^{57}Fe (0.005), ^{65}Cu (0.005), ^{66}Zn (0.005), ^{206}Pb (0.01), ^{207}Pb (0.01), ^{208}Pb (0.01). In this analysis, no quantification of Pb was conducted due to lack of suitable reference materials for calibration, however intensity of Pb (and other elements) was normalized to ^{13}C (carbon) intensity as Wu et al. (2009), Johnston et al. (2019) and others have utilized to normalize the ablation efficiency. Detailed analytical conditions are presented in supplementary Table S3. From the continuous list of raw pixel values data, elemental images were reconstructed using LA-ICP-MS Image generator house-made software iQquant2 (Kawakami et al., 2016).

177

178 **2.4. Immunohistochemistry**

179 Immunohistochemistry (IHC) was carried out using the method described by
180 Skibinska-Kijek et al. (2009) and Wang et al. (2010) with minor modifications. Sections
181 of the embedded liver, kidney, and brain samples were cut on a cryostat to a thickness of
182 20 μm. After fixation with 4% paraformaldehyde phosphate buffer solution and
183 quenching of endogenous peroxidase activity with 0.3% H_2O_2 in methanol, the sections
184 were blocked with goat serum in Phosphate Buffered Saline (PBS). Then, the sections
185 were incubated overnight at 4°C with antibody recognizing STIM1 (ProteinTech Group
186 Inc., cat no 11565-1-AP, the antibody was raised against an N-terminal fragment of the
187 protein: aa 2-350) diluted 1:200 in PBS. Samples were then washed and incubated with
188 biotinylated secondary antibodies (Vector Laboratories, Burlingame, CA, USA) in PBS
189 for thirty minutes. After washing, the sections were incubated with Avidin-biotin
190 complex reagent (ABC-Elite kit, Vector Laboratories), following the manufacturers
191 protocol. The immunocomplex was visualized with diaminobenzidine (DAB) (Vector
192 Laboratories), sections were counterstained with haematoxylin (Sigma-Aldrich), and
193 observations were conducted by microscope (BIOREVO BZ-9000 series; KEYENCE,
194 Osaka, Japan).

195

196 **2.5. Quantitative analysis by real time PCR**

197 Real time PCR was performed using the method described by Skibinska-Kijec
198 et al. (2009) with small modifications. Total RNA was extracted from small pieces of
199 liver, kidney, and brain soaked in RNAlater (Sigma-Aldrich) using Nucleo spin (Takara
200 bio, Shiga, Japan). First-strand cDNA was generated from 600 ng of total RNA in a

final volume of 20 μL with ReverTra Ace (Toyobo, Osaka, Japan). This was examined by real time PCR with specific gene primers for *Stim1* (NM_009287; (5'GCTCTCAATGCCATGCCTTCCAAT, 5'TCTAGGCCATGGTTCAACGCCATA), and Fast SYBR Green Master mix (Applied Biosystems). The samples were analyzed using 7000 Sequence Detection System hardware and software (Applied Biosystems). *18S ribosomal RNA* (NR_003278) for normalization was used with the following primers: 5'AACGAACGAGACTCTGGCATG and 5'CGGACATCTAAGGGCATCACA. A relative quantification (RQ) method was used to calculate the relative levels of *Stim1* mRNA. The formula was as follows: RQ = $2^{-deltaCT}$, where deltaCT = CT(target) – CT(18S). Amplification efficiency was 98.0% for *STIM1* and 100.5% for *18S ribosomal RNA*.

2.6. Microarray analysis

To analyze gene expression profiles, a microarray experiment was performed. Firstly, the total RNA of the liver, kidney, and brain was quantified and qualified using an Agilent 2100 Bioanalyzer series II (Agilent Technologies, supplementary Table S4). Cyanine 3-labelled cRNA was prepared from 500 ng of total RNA, and amplified using a Low Input Quick Amp Labeling Kit (Agilent Technologies), according to the manufacturer's instructions, followed by RNAeasy column purification (Qiagen, Valencia, CA). Dye incorporation and cRNA yield were checked with the NanoDrop ND-1000 Spectrophotometer the Agilent 2100 Bioanalyzer. Gene Expression (GE) Hybridization Kit (Agilent Technologies) was used for labeling. 600 ng of Cy3-labelled cRNA was fragmented at 60°C for 30 minutes following the manufacturer's instructions. On completion of the fragmentation reaction, 25 μL of 2x Agilent hybridization buffer

225 was added to the fragmentation mixture and hybridized to Agilent SurePrint G3 Mouse
226 8 x 60K ver.2.0 for 17 hours at 65°C in a rotating Agilent hybridization oven. After
227 hybridization, slides were washed 1 minute at room temperature with GE Wash Buffer 1
228 (Agilent) and 1 minute with 37°C GE Wash buffer 2 (Agilent), then air-dried
229 immediately. Slide was scanned immediately after washing on the Agilent DNA
230 Microarray Scanner using one color scan setting (Agilent Technologies, Scan
231 Resolution; 3 μm, TIFF file dynamic range; 20bit). The scanned images were analyzed
232 with Feature Extraction Software 12.0.3.1 (Agilent) using default parameters to obtain
233 background subtracted and spatially detrended Processed Signal intensities. Normalized
234 (75 Percentile Shift) signal intensity was used for data acquisition. The data for
235 microarray is deposited at the NCBI Gene Expression Omnibus (GEO) database;
236 accession number is “Series GSE93544”.
237
238 **2.7. Statistical analysis**
239 All statistical analyses were carried out using JMP 12 (SAS Institute, Cary, NC,
240 USA). A Tukey-Kramer test was performed to compare body weights, Pb concentration,
241 and gene expression of STIM1 in tissue samples between groups. All statistical analyses
242 were performed at a significance level of 95%.
243

3. Results

3.1. Pb concentrations in mice organs

Table 1 shows the mean ± standard deviations (SD) of the Pb concentration in the blood, liver, kidney, and brain of the three groups. A dose dependent increase of Pb concentration in the organs was observed and there were significant differences in Pb concentration in the blood and all tissue-types between the control and high Pb dosage groups.

3.2. Pb local distributions in mice organs

The local distribution of Pb in the liver, kidney, and brain of the three mice groups are shown in Figures 1, 2, and 3, respectively. A homogeneous distribution of Pb was found in the liver of the low and high dosage groups (Figure 1). Yet surprisingly, inhomogeneous Pb distribution was discovered in the kidney and brain (Figures 2 and 3). Within the kidney, in the internal area surrounding the medulla there was a higher regional Pb concentration than in the renal cortex in the low and high dosage groups (Figure 2). The brain also showed an inhomogeneous distribution; the hippocampus had higher Pb concentration than other areas such as the white matter in high dosage group (Figure 3). Pb in all tissues of the control group and in the brain of the low dosage group was not detected as count values of ICP-MS were comparable to those of background areas where only glass slide without organs (Figure 3). Additionally, other elements distribution are shown in supplementary Figure S2. For example, Mn tended to accumulate in the renal medulla than cortex (supplementary Figure S2 (D, E, F)), while selective accumulation of Zn was observed in the hippocampus of brain (supplementary

Figure S2 (G, H, I)). These results were in accordance with the previous studies (Becker et al., 2010, Shariatgorji et al., 2016).

3.3. Immuno-localization of STIM1 in mice organs

The reactivity of the primary antibody was confirmed by comparing it with PBS (supplementary Figure S3). Figures 1, 2, and 3 show the immune-localization of STIM1 in the liver, kidney, and brain of the three groups, respectively. A homogeneous distribution of STIM1 was found in the liver and kidney in all groups (Figures 1 and 2). However, the brain showed inhomogeneous distribution of STIM1: the gray matter and hippocampus had higher densities than other areas such as the white matter in all groups (Figure 3).

3.4. Gene induction by Pb in mice organs

Real time PCR was performed to measure the levels of STIM1 mRNA in the liver, kidney, and brain. This confirmed that STIM1 was expressed in all organs (Figure 4). However, there were no significant differences in gene expression between groups in any of the organs. Additionally, it was examined gene induction of the candidates suspected to be responsible for Pb entry into cells such as STIM1, Orai1, TRP, VGCC, divalent metal transporter 1, and anion exchanger in the liver, kidney, and brain by microarray. However, no significant induction was observed in the liver, kidney, and brain. As a confirmation, the induction of metallothionein, which is known to be induced with Pb exposure, was observed to be two and eight times greater in the liver and kidney, respectively, in the high dosage groups compared with the control group (data not shown).

4. Discussion

4.1. Pb local distribution in organs

The local distribution of Pb and other toxic elements in organs is still unknown. LA-ICP-MS allows direct analysis of thin organ sections (Becker et al., 2010). However, as for Pb, there is little published research regarding bioimaging, especially in the Pb exposed mice model.

In the present study, Pb concentration found in kidney (56.65 mg/kg) and liver (16.49 mg/kg) in high dosage groups were comparable to that for lead-poisoned animals in the previous study (Takano et al., 2015). By analysis using LA-ICP-MS, a homogenous Pb distribution was found in the liver (Figure 1); however, the kidney and brain showed inhomogeneous distribution of Pb (Figures 2 and 3) mainly in the kidney. Since it was identified as a target soft tissue for Pb accumulation (Barregard et al., 1999), there has been substantial research published on Pb concentration in animal kidneys (Yabe et al., 2012, 2013, Bortey-Sam et al., 2015, Jarzynska et al., 2011, Nakayama et al., 2011, 2013, Sedki et al., 2003). These reports were based on the hypothesis that there is a homogenous distribution of Pb in the kidney, and thus did not map the element in this organ. However, the present findings suggest that such mapping should be considered for identifying toxic elements in the kidney. As Pb and other types of toxic elements are mainly observed in the proximal tubule, which is primarily distributed in the cortex, the proximal tubule was regarded to be the highest accumulation area in the kidney (Sabolic 2006). Moreover, there are some reports about studies focusing toxic elements distribution in the renal cortex (Smith et al., 1991, Wang et al., 2009, Wlostowski et al., 2006), so, to some extent, it might be reasonable to focus such region. A previous study using LA-ICP-MS to determine Pt in cisplatin

(Pt)-administrated rats found that Pt tended to accumulate in the cortex and corticomedullary junction (Moreno-Gordaliza et al., 2011). However, the results of the present study which revealed that Pb tended to accumulate in the medulla rather than the cortex, strongly suggest that high sensitivity areas and high accumulation areas differ. The present study would help to understand mechanism of pathological Pb toxicity.

Differences in Pb distribution among organs may be explained by their individual characteristics. In histological anatomy and physiology, the liver is regarded as a homogenous organ, thus Pb is distributed homogenously. By contrast, the kidneys and brain are regarded as inhomogeneous organs, therefore Pb is distributed inhomogeneously.

In the present study, mice were selected to be the first proof of concept model, yet the method utilized can be applied to other animals. For instance, previous research has shown the tolerance of chickens to chronic Pb intoxication (Mazliah et al., 1989); thus, revealing local distribution of Pb in chicken organs would be interesting.

4.2. Comparison between Pb and STIM1 distribution and gene expression of STIM1

The present study found homogeneous distribution of STIM1, which is the main component of SOCs, in the liver and kidney, whereas there was inhomogeneous distribution in the brain (Figures 1, 2, and 3). There was a significant difference between the distribution of Pb and STIM1 in the kidney which suggests that there are alternative mechanisms underlying Pb distribution in the kidney. One explanation is that Pb distribution is due to its reabsorption. In the kidney, Pb is filtered in the glomerulus; however, most of this filtered Pb is reabsorbed by the distal tubule and the collecting

duct (Araki et al., 1983, 1978). The distal tubule and the collecting duct are primarily located in the renal medulla, the area which had the highest concentration of Pb compared with the other areas analyzed in the present study. As for channels and transporters, the TRP super family, specifically TRP vanilloid (TRPV) 5, is responsible for transcellular calcium (Ca^{2+}) reabsorption in the distal tubule, connecting tube, and collecting duct of the kidney (Nijenhuis et al., 2005). Moreover, the Na^{+}-Ca^{2+} exchanger (NCX) and plasma membrane Ca^{2+} ATPase (PMCA) are responsible for the extrusion of Ca^{2+} into the blood (Hoenderop et al., 2000). Despite the fact that there have not been any studies revealing linkages between these transporters and Pb distribution, these transporters might also be responsible for Pb^{2+} reabsorption and local distribution in the kidney. Moreover, reabsorption behavior differs between Pb and other toxic metals such as Cd, Hg (Araki et al., 1986); thus further study of transporters and other toxic elements could be a key to support the idea proposed above.

In the brain, STIM1 is mainly distributed in the hippocampus, which is similar with Pb distribution. Therefore, SOCs may be a candidate route for Pb entering brain cells. However, VGCCs in the brain may also be a feasible candidate, as nerve cells are excitable (Davila et al., 1999, Vassanelli and Fromherz 1998). Additionally, no induction of STIM1 expression by Pb was observed in the current study, suggesting that Pb enters the cells via other mechanisms.

5. Conclusions

In experimental animals such as mice model, local distribution of Pb was demonstrated for liver, kidney and brain and compared with the distribution of Pb and STIM1 for the first time. Inhomogeneous distribution of Pb was found in the kidney and

363 brain. In the kidney, Pb tended to accumulate in the medulla rather than the cortex. This
364 provides support for the mechanism of Pb toxicity as the proximal tubule is regarded as
365 an area of high accumulation. In this study, however, we did not find evidence
366 supporting that Pb enters the cells via SOCs. Thus, further study should be conducted to
367 elucidate the local distribution of Pb and other toxic elements, and pathway that Pb
368 takes to the cells.
369
370
371 **Acknowledgements**
372 The analyses were technically supported by Mr. Takahiro Ichise, Ms. Mio
373 Yagihashi and Ms. Nagisa Hirano. The English in this manuscript was proofread by
374 uni-edit (https://uni-edit.net/usa).
375 This work was supported by Grants-in-Aid for Scientific Research from the
376 Ministry of Education, Culture, Sports, Science and Technology of Japan awarded to M.
377 Ishizuka (No. 16H0177906, 18K1984708) and Y. Ikenaka (17K2003807, 18H0413208),
378 and S.M.M. Nakayama (No. 16K16197, 17KK0009), and the foundation of JSPS Core
379 to Core Program (AA Science Platforms), the Environment Research and Technology
380 Development Fund (SII-1/3-2, 4RF-1802/18949907) of the Environmental Restoration
381 and Conservation Agency of Japan. We also acknowledge financial support from The
382 Soroptimist Japan Foundation, The Nakajima Foundation, The Sumitomo foundation,
383 The Nihon Seimei Foundation and The Japan Prize Foundation. This research was also
384 supported by JST/JICA, SATREPS (Science and Technology Research Partnership for
385 Sustainable Development).
386

Conflict of interest

The authors declare no conflict of interest in this study.

Author Contributions

M.T., S.M.M.N., Y.M., Y.I., K.Y., T.H., and M.I. conceived and designed the experiments; M.T., S.M.M.N., Y.M., A.K., and M.T. performed the experiments; M.T., S.M.M.N., and H.M. analyzed the data; M.T., S.M.M.N., Y.M. and M.I. have written the manuscript; all authors have read and approved the final manuscript.

Supplementary material

Detailed information related to this study are available as supplementary material.

Figure captions

Figure 1. Distribution of ^{208}Pb and STIM1 in a 20 μm section of liver. Distribution of $^{208}Pb/^{13}C$ analyzed by LA-ICP-MS (left). STIM1 was analyzed by IHC (right). Scale bar is 3 mm. Among LA-ICP-MS images, the scale bar indicates the ratio of intensity ($^{208}Pb/^{13}C$).

Figure 2. Distribution of ^{208}Pb and STIM1 in a 20 μm section of kidney. Distribution of $^{208}Pb/^{13}C$ analyzed by LA-ICP-MS (left). STIM1 was analyzed by IHC (right). Scale bar is 3 mm. Among LA-ICP-MS images, the scale bar indicates the ratio of intensity ($^{208}Pb/^{13}C$).

Figure 3. Distribution of ^{208}Pb and STIM1 in a 20 μm section of brain. Distribution of $^{208}Pb/^{13}C$ analyzed by LA-ICP-MS (left). STIM1 was analyzed by IHC (right). Scale bar is 5 mm. Among LA-ICP-MS images, the scale bar indicates the ratio of intensity ($^{208}Pb/^{13}C$).

Figure 4. Mean ± SD of the expression of STIM1 in mice organs in the three dosage groups: (A) liver, (B) kidney, and (C) brain. No significant differences were found between groups.

References

Araki S. The effects of water restriction and water loading on urinary excretion of lead, delta-aminolevulinic acid and coproporphyrin, Br J Ind Med 35 (1978) 312-317.

Araki S., Aono H., Yokoyama K., Murata K. Filterable plasma concentration, glomerular filtration, tubular balance and renal clearance of heavy materials and organic substances in metal workers, Arch Environ Health 41 (1986) 216-221.

Araki S., Murata K., Yokoyama K., Yanagihara S., Niinuma Y., Yamamoto R., Ishihara N. Circadian rhythms in the urinary excretion of metals and organic substances in 'healthy' men, Arch Environ Health 38 (1983) 360-366.

Barregard L., Svalander C., Schutz A., Westberg G., Sallsten G., Blohme I., Molne J., Attman P.O., Haglind P. Cadmium, mercury, and lead in kidney cortex of the general Swedish population: A study of biopsies from living kidney donors, Environ. Health Perspect. 107 (1999) 867-871.

Becker J.S. Recent developments in isotope analysis by advanced mass spectrometric techniques Plenary lecture, J. Anal. At. Spectrom. 20 (2005) 1173-1184.

Becker J.S., Breuer U., Hsieh H.F., Osterholt T., Kumtabtim U., Wu B., Matusch A., Caruso J.A., Qin Z.Y. Bioimaging of metals and biomolecules in mouse heart by laser ablation inductively coupled plasma mass spectrometry and secondary ion mass spectrometry, Anal. Chem. 82 (2015) 9528-9533.

Becker J.S., Zoriy M., Matusch A., Wu B., Salber D., Palm C. Bioimaging of metals by laser ablation inductively coupled plasma mass spectrometry (LA-ICP-MS), Mass Spectrom. Rev. 29 (2010) 156-175.

Bortey-Sam N., Nakayama S.M.M., Ikenaka Y., Akoto O., Baidoo E., Yohannes Y.B., Mizukawa H., Ishizuka M. Human health risks from metals and metalloid via consumption of food animals near gold mines in Tarkwa, Ghana: Estimation of the daily intakes and target hazard quotients (THQs), Ecotoxicol. Environ. Saf. 111 (2015) 160-167.

Chang Y. F., Teng H. C., Cheng S. Y., Wang C. T., Chiou S. H., Kao L. S., Kao F. J., Chiou A., Yang D.M. Orai1-STIM1 formed store-operated Ca2+ channels (SOCs) as the molecular components needed for Pb2+ entry in living cells, Toxicol. Appl. Pharmacol. 227 (2008) 430-439.

Cheng K.T., Liu X.B., Ong H.L., Ambudkar I.S. Functional requirement for Orai1 in store-operated TRPC1-STIM1 channels, J. Biol. Chem. 283 (2008) 12935-12940.

Chiu T.Y., Teng H.C., Huang P.C., Kao F.J., Yang D.M. Dominant role of Orai1 with STIM1 on the cytosolic entry and cytotoxicity of lead ions, Toxicol. Sci. 110 (2009) 353-362.

Davila H.M. Molecular and functional diversity of voltage-gated calcium channels, Ann. N. Y. Acad. Sci. 868 (1999) 102-117.

Dobrowolska J., Dehnhardt M., Matusch A., Zoriy M., Palomero-Gallagher N., Koscielniak P., Zilles K., Becker J.S. Quantitative imaging of zinc, copper and lead in three distinct regions of the human brain by laser ablation inductively coupled plasma mass spectrometry, Talanta 74 (2008) 717-723.

Godwin H.A. The biological chemistry of lead, Curr Opin Chem Biol 5 (2001) 223-227.

Hoenderop J.G.J., Hartog A., Stuiver M., Doucet A., Willems P., Bindels R.J.M. Localization of the epithelial Ca2+ channel in rabbit kidney and intestine, J. Am. Soc. Nephrol. 11 (2000) 1171-1178.

Ishii C., Nakayama S.M.M., Kataba A., Ikenaka Y., Saito K., Watanabe Y., Makino Y., Matsukawa T., Kubota A., Yokoyama K., Mizukawa H., Hirata T., Ishizuka M. Characterization and imaging of lead distribution in bones of lead-exposed birds by ICP-MS and LA-ICP-MS, Chemosphere 212 (2018) 994-1001.

Jarzynska G, Falandysz J. Selenium and 17 other largely essential and toxic metals in muscle and organ meats of Red Deer (Cervus elaphus) - Consequences to human health, Environ. Int. 37 (2011) 882-888.

500 Johnston, J.E., Franklin M., Roh H., Austin C., Arora. Lead and Arsenic in Shed
501 Deciduous Teeth of Children Living Near a Lead-Acid Battery Smelter. Environ. Sci.
502 Technol. 53 (2019) 6000-6006.
503
504 Kawakami T., Hokada T., Sakata S., Hirata T. Possible polymetamorphism and brine
505 infiltration recorded in the garnet-sillimanite gneiss, Skallevikshalsen, Lutzow-Holm
506 Complex, East Antarctica, J. Mineral. Petrol. Sci. 111 (2016) 129-143.
507
508 Kerper L.E., Hinkle P.M. Cellular uptake of lead is activated by depletion of
509 intracellular calcium stores, J. Biol. Chem. 272 (1997) 8346-8352.
510
511 Klejman M.E., Gruszczynska-Biegala J., Skibinska-Kijek A., Wisniewska M.B., Misztal
512 K., Blazejczyk M., Bojarski L., Kuznicki J. Expression of STIM1 in brain and
513 puncta-like co-localization of STIM1 and ORAI1 upon depletion of Ca2+ store in
514 neurons, Neurochem. Int. 54 (2009) 49-55.
515
516 Konz I., Fernandez B., Fernandez M.L., Pereiro R., Sanz-Medel A. Laser ablation
517 ICP-MS for quantitative biomedical applications, Anal. Bioanal. Chem. 403 (2012)
518 2113-2125.
519
520 Liao Y., Erxleben C., Abramowitz J., Flockerzi V., Zhu M.X., Armstrong D.L.,
521 Birnbaumer L. Functional interactions among Orai1, TRPCs, and STIM1 suggest a
522 STIM-regulated heteromeric Orai/TRPC model for SOCE/Icrac channels, Proc. Natl.
523 Acad. Sci. U.S.A. 105 (2008) 2895-2900.

Limbeck A., Galler P., Bonta M., Bauer G., Nischkauer W., Vanhaecke F. Recent advances in quantitative LA-ICP-MS analysis: challenges and solutions in the life sciences and environmental chemistry, Anal. Bioanal. Chem. 407 (2015) 6593-6617.

Mazliah J., Barron S., Bental E., Rogowski Z., Coleman R., Silbermann M. The effects of long-term lead intoxication on the nervous system of the chicken, Neurosci. Lett. 101 (1989) 253–257.

Moreno-Gordaliza E., Giesen C., Lazaro A., Esteban-Fernandez D., Humanes B., Canas B., Panne U., Tejedor A., Jakubowski N., Gomez-Gomez M.M. Elemental bioimaging in kidney by LA-ICP-MS as a tool to study nephrotoxicity and renal protective strategies in cisplatin therapies. Anal. Chem. 83 (2011) 7933-7940.

Nakata H., Nakayama S.M.M., Ikenaka Y., Mizukawa H., Ishii C., Yohannes Y.B., Konnai S., Darwish W.S., Ishizuka M. Metal extent in blood of livestock from Dandora dumping site, Kenya: Source identification of Pb exposure by stable isotope analysis, Environ. Pollut. 205 (2015) 8-15.

Nakata H., Nakayama S.M.M., Yabe J., Liazambi A., Mizukawa H., Darwish W.S., Ikenaka Y., Ishizuka M. Reliability of stable Pb isotopes to identify Pb sources and verifying biological fractionation of Pb isotopes in goats and chickens, Environ. Pollut. 208 (2016) 395-403.

548 Nakayama S.M.M., Ikenaka Y., Hamada K., Muzandu K., Choongo K., Teraoka H.,
549 Mizuno N., Ishizuka M. Metal and metalloid contamination in roadside soil and wild
550 rats around a Pb-Zn mine in Kabwe, Zambia, Environ. Pollut. 159 (2011) 175-181.
551
552 Nakayama S.M.M., Ikenaka Y., Hamada K., Muzandu K., Choongo K., Yabe J.,
553 Umemura T., Ishizuka M. Accumulation and biological effects of metals in wild rats in
554 mining areas of Zambia, Environ Monit Assess 185 (2013) 4907-4918.
555
556 Nijenhuis T., Hoenderop J.G.J., Bindels R.J.M. TRPV5 and TRPV6 in Ca2+
557 (re)absorption: regulating Ca2+ entry at the gate, Pflugers Arch. 451 (2005) 181-192.
558
559 Noël M., Christensen J.R., Spence J., Robbins C.T. Using laser ablation inductively
560 coupled plasma mass spectrometry (LA-ICP-MS) to characterize copper, zinc and
561 mercury along grizzly bear hair providing estimate of diet. Sci Total Environ. 529
562 (2015) 1-9
563
564 Paul B., Hare D.J., Bishop D.P., Paton C., Nguyen V.T., Cole N., Niedwiecki M.M.,
565 Andreozzi E., Vais A., Billings J.L., Bray L., Bush A.I., McColl G., Roberts B.R.,
566 Adlard P.A., Finkelstein D.I., Hellstrom J., Hergt J.M., Woodhead J.D., Doble P.A.
567 Visualising mouse neuroanatomy and function by metal distribution using laser
568 ablation-inductively coupled plasma-mass spectrometry imaging, Chem. Sci. 6 (2015)
569 5383-5393.
570

Pozebon D., Scheffler G.L., Dressler V.L., Nunes M.A. Review of the applications of laser ablation inductively coupled plasma mass spectrometry (LA-ICP-MS) to the analysis of biological samples, J. Anal. At. Spectrom. 29 (12) (2014) 2204-2228.

Rahil-Khazen R., Bolann B.J., Myking A., Ulvik R.J. Multi-element analysis of trace element levels in human autopsy tissues by using inductively coupled atomic emission spectrometry technique (ICP-AES), J Trace Elem Med Biol 16 (2002) 15-25.

Sabolic I. Common mechanisms in nephropathy induced by toxic metals, Nephron Physiol 104 (2006) 107-114.

Sedki A., Lekouch N., Gamon S., Pineau A. Toxic and essential trace metals in muscle, liver and kidney of bovines from a polluted area of Morocco, Sci. Total Environ. 317 (2003) 201-205.

Shariatgorji M., Nilsson A., Bonta M., Gan J.R., Marklund N., Clausen F., Kallback P., Loden H., Limbeck A., Andren P.E. Direct imaging of elemental distributions in tissue sections by laser ablation mass spectrometry, Methods 104 (2016) 86-92.

Skibinska-Kijek A., Wisniewska M.B., Gruszczynska-Biegala J., Methner A., Kuznicki J., Immunolocalization of STIM1 in the mouse brain, Acta Neurobiol. Exp. 69 (2009) 413-428.

Smith R.M., Griel L.C., Muller L.D., Leach R.M., Baker D.E. Effects of dietary cadmium chloride throughout gestation on blood and tissue metabolites of primigravid and neonatal dairy cattle, J. Anim. Sci. 69 (1991) 4078-4087.

Takano T., Okutomi Y., Mochizuki M., Ochiai Y., Yamada F., Mori M., Ueda F. Biological index of environmental lead pollution: accumulation of lead in liver and kidney in mice, Environ Monit Assess 187 (2015) 1-5.

Urgast D.S., Ou O., Gordon M.J., Raab A., Nixon G.F., Kwun I.S., Beattie J.H., Feldmann J. Microanalytical isotope ratio measurements and elemental mapping using laser ablation ICP-MS for tissue thin sections: zinc tracer studies in rats, Anal. Bioanal. Chem. 402 (2012) 287-297.

Vassanelli S., Fromherz P. Transistor records of excitable neurons from rat brain, Appl Phys A Mater Sci Process 66 (1998) 459-463.

Wang L., Chen D.W., Wang H., Liu Z.P. Effects of lead and/or cadmium on the expression of metallothionein in the kidney of rats, Biol Trace Elem Res 129 (2009) 190-199.

Wang L.M., Becker J.S., Wu Q., O M.F., Bliveira M.F., Bozza F.A., Schwager A.L., Hoffman J.M., Morton K.A. Bioimaging of copper alterations in the aging mouse brain by autoradiography, laser ablation inductively coupled plasma mass spectrometry and immunohistochemistry. Metallomics. 2 (2010) 348-353.

Wlostowski T., Bonda E., Krasowska A. Free-ranging European bisons accumulate more cadmium in the liver and kidneys than domestic cattle in north-eastern Poland, Sci. Total Environ. 364 (2006) 295-300.

Wu B., Zoriy M., Chen Y., Becker J.S. Imaging of nutrient elements in the leaves of Elsholtzia splendens by laser ablation inductively coupled plasma mass spectrometry (LA-ICP-MS), Talenta. 78 (2009) 132-137.

Yabe J., Nakayama S.M.M., Ikenaka Y., Muzandu K., Choongo K., Mainda G., Kabeta M., Ishizuka M., Umemura T. Metal distribution in tissues of free-range chickens near a lead-zinc mine in Kabwe, Zambia, Environ. Toxicol. Chem. 32 (2013) 189-192.

Yabe J., Nakayama S.M.M., Ikenaka Y., Muzandu K., Ishizuka M., Umemura T. Accumulation of metals in the liver and kidneys of cattle from agricultural areas in Lusaka, Zambia, J. Vet. Med. Sci. 74 (2012) 1345-1347.

Yamashita S., Yoshikuni Y., Obayashi H., Suzuki T., Green D., Hirata T. Simultaneous Determination of Size and Position of Silver and Gold Nanoparticles in Onion Cells using Laser Ablation-ICP-MS. Anal. Chem. 91. (2019) 4544-4551.

Zhang H., Li W., Xue Y., Zou F. TRPC1 is involved in Ca2+ influx and cytotoxicity following Pb2+ exposure in human embryonic kidney cells, Toxicol. Lett. 229 (2014) 52-58.

Table 1. Mean ± SD of the Pb concentration in the blood and organs of mice for the three dosage groups.

	Control	Low	High
Blood (μg/dL)	1.8 ± 0.5^{a}	14.9 ± 3.2^{b}	40.8 ± 3.9^{c}
Liver (mg/kg)	0.016 ± 0.001^{a}	4.54 ± 0.59^{b}	16.49 ± 1.58^{c}
Kidney (mg/kg)	0.044 ± 0.002^{a}	11.47 ± 1.48^{a}	56.65 ± 20.20^{b}
Brain (mg/kg)	0.027 ± 0.008^{a}	0.54 ± 0.09^{b}	2.66 ± 0.33^{c}

Note:

Different letters (a, b, and c) between columns indicate a significant difference between dosage groups ($p < 0.05$).

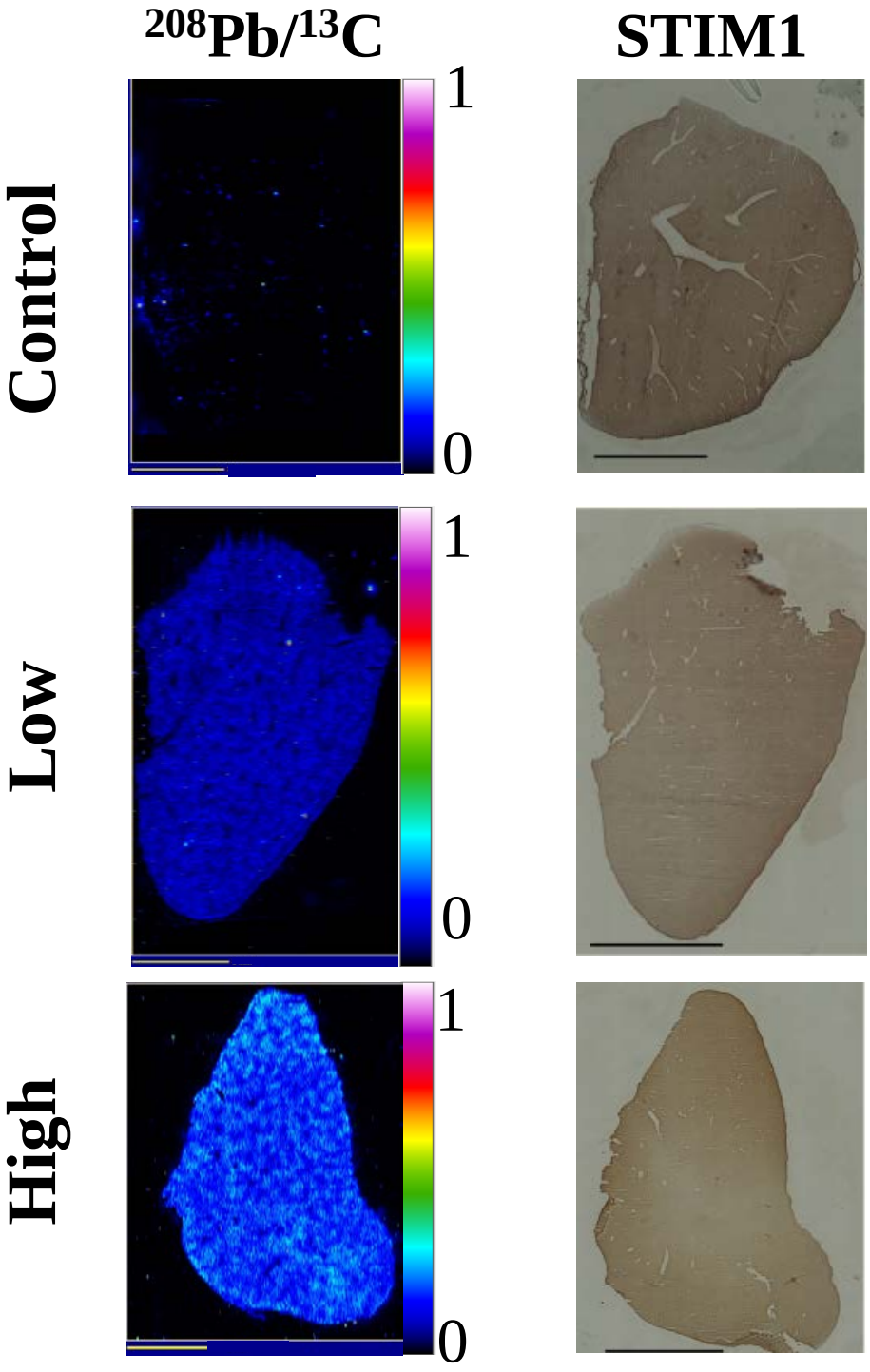

Figure 1.

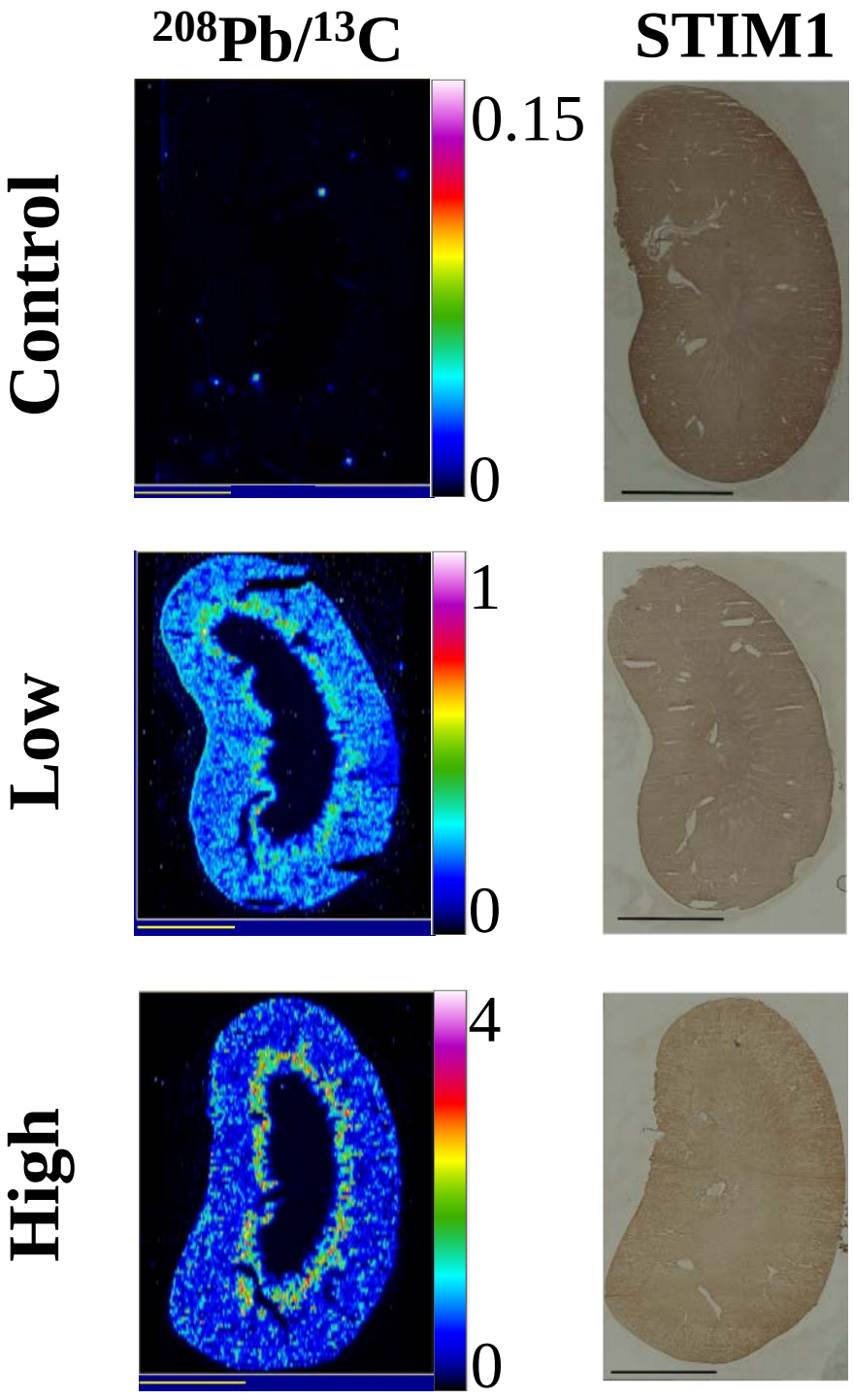

Figure 2.

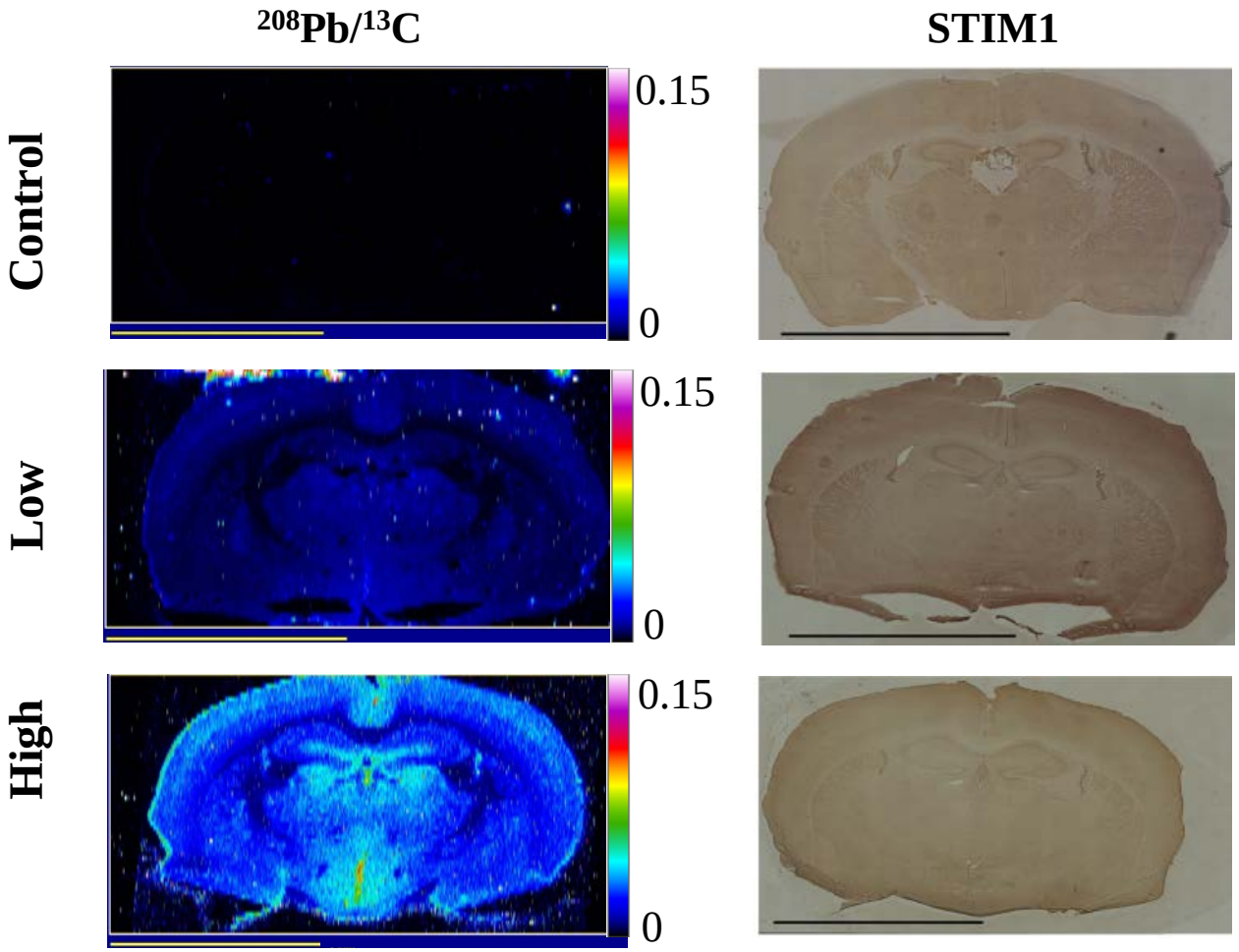

Figure 3.

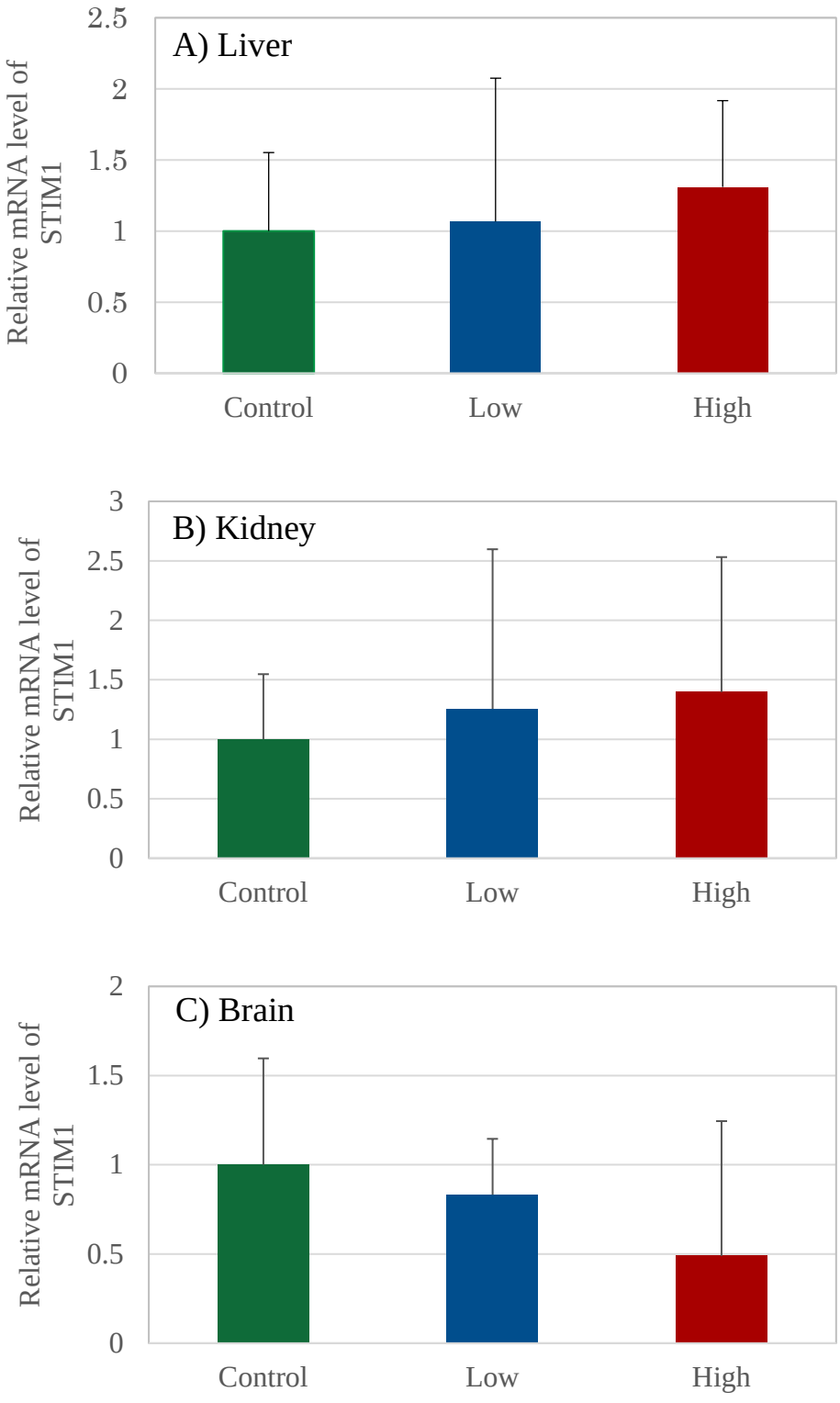
A) Liver
Relative mRNA level of STIM1
2.5
2
1.5
1
0.5
0
Control
Low
High
B) Kidney
Relative mRNA level of STIM1
3
2.5
2
1.5
1
0.5
0
Control
Low
High
C) Brain
Relative mRNA level of STIM1
2
1.5
1
0.5
0
Control
Low
High

Figure 4.